Crystallographic Facet Selective HER Catalysis: Exemplified in FeP and NiP_2 Single Crystals

Bryan Owens-Baird,[1,2] Juliana P. S. Sousa,[3] Yasmine Ziouani,[3] Dmitri Petrovykh,[3] Nikolai A. Zarkevich,[2] Duane D. Johnson,[2,4] Yury V. Kolen'ko,[3,*] Kirill Kovnir[1,2,*]

[1] Department of Chemistry, Iowa State University, Ames, IA, 50011 USA

[2] Ames Laboratory, U.S. Department of Energy, Ames, IA, 50011 USA

[3] Nanochemistry Research Group, International Iberian Nanotechnology Laboratory, Braga 4715-330, Portugal

[4] Department of Materials Science & Engineering, Iowa State University, Ames, IA, 50011 USA

E-mail: kovnir@iastate.edu

Supporting Information

Single crystal X-ray diffraction characterization: The synthesized single crystals were analyzed and facet-indexed through single-crystal X-ray diffraction (SC–XRD) carried out using a Bruker D8 Venture diffractometer with a Bruker Photon100 CMOS detector and employing Mo-K_α radiation (λ = 0.71073 Å) for the facet indexing of multiple FeP and *m*-NiP_2 crystals. Facet indexing was conducted at room temperature, with frames for each crystal collected in 2° increments over the full 360° range for φ. The detector was located close to the X-ray source, collecting diffraction spots arising from back-diffraction, which is often necessary as the absorption from large crystals was too high to allow for transmission diffraction.

Structural sensitivity of electrocatalytic properties: The HER catalytic activity of FeP and *m*-NiP_2 crystals were measured in 0.5 M H_2SO_4 electrolyte using a three-electrode setup, with the counter electrode being graphite and a saturated calomel electrode (SCE) reference electrode (Figure 2b). To ensure that only the desired facet was exposed to the solution, the crystal was dipped into the electrolyte and then raised slightly. This formed a meniscus around the perimeter of the crystal face. Electrochemical measurements were conducted using a Metrohm Autolab PGSTAT302N potentiostat. The surface area of the studied facet was calculated with high precision using electronic optical microscope.

X-ray photoelectron spectroscopy (XPS): XPS measurements were performed using a monochromated micro-focused Al-K_α X-ray source that defined an analysis spot of ca. 650×400 μm^2. All spectra were acquired in normal emission with an enabled magnetic lens, producing an effective analyzer collection angle of ca. 30°. Elemental regions were acquired at the nominal instrument resolution of 0.36 eV, with 0.1 eV step size. The binding energy (BE) scale of the analyzer had been calibrated based on Au $4f_{7/2}$ reference BE value of 83.95 eV.[1] For the *m*-NiP_2 sample, charge neutralization was provided by beams of low-energy (≤10 eV) Ar^+ ions and electrons guided by the magnetic lens. For the FeP sample, charge neutralization was not necessary. Both samples were measured after catalytic testing had been performed. The symmetric peak shapes and FWHM as low as 0.6 eV (for resolved P 2p doublets) implied a uniform charge neutralization and the high chemical uniformity of the bulk crystalline materials. The aliphatic C 1s peak was observed at BE of 284.7 ± 0.1 eV for all samples, in agreement with previous measurements of nanostructured catalysts,[2-4] indicating that the measured BE values can be directly compared to the ones from the literature. Notably, the typical aliphatic C 1s BEs tend to be in a slightly higher range of 285.0 ± 0.2 eV for samples where the corresponding adventitious[5-6] or organic[7-8] carbon layer is measured on semi-metallic or doped semiconductor materials with low-to-minimal surface oxidation and crystalline conductive bulk. Accordingly, the observed aliphatic C 1s BE range is consistent with an adventitious carbon layer on top of a significant oxidized surface overlayer, to remove which depth profiling was performed using Ar clusters at 6000 eV, in cycles of 60 s (30 s for the first 7 cycles on FeP sample); the Ar cluster beam was chosen to minimize the potential damage to the underlying crystalline materials.[9]

A convolution of Lorentzian and Gaussian line shapes on a linear combination of Shirley and linear backgrounds was used to fit the individual components, choosing the minimal number of self-consistent components that were able to fit spectra across the depth-profile set for each sample. An asymmetric line shape was used to fit the metallic component in Fe $2p_{3/2}$ region. The reported elemental ratios were estimated from the standard “atomic %” elemental compositions that were quantified using calibrated analyzer transmission functions, Scofield sensitivity factors,[10] and effective attenuation lengths (EALs) for photoelectrons.[11] EALs for elemental ratios and film thickness estimates were calculated using the standard TPP-2M formalism,[11-12] as implemented in Avantage software (Thermo Scientific).

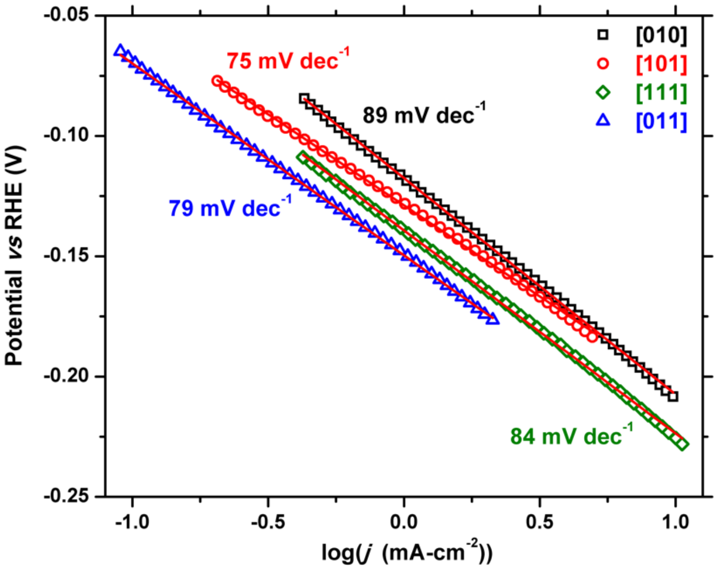

Figure S1. Tafel slopes of FeP (fitted) for the [010], [101], [111], and [011] facets.

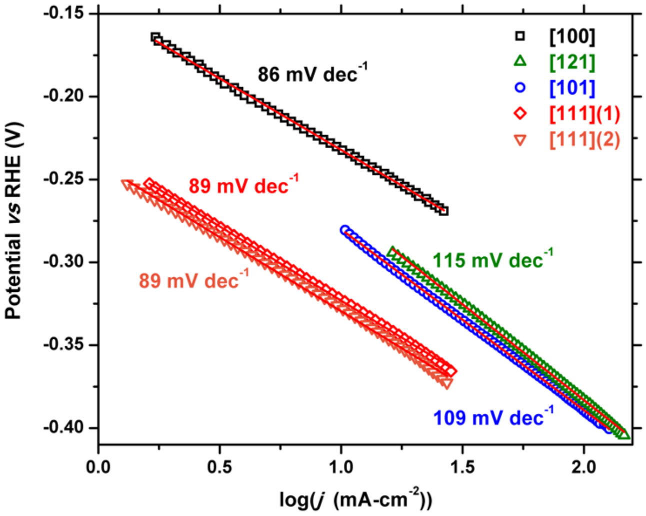

Figure S2. Tafel slopes of *m*-NiP_2 (fitted) for [100], [121], [101], $[111]_1$, and $[111]_2$ facets.

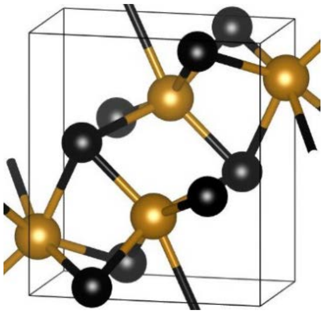

Figure S3. FeP (*Pnma* $D2_h$-16) bulk structure with a = 5.152 Å, b=3.046 Å, and c=5.761 Å. Atoms are denoted by spheres for Fe (orange) and P (black); while the unit cell is shown by grey lines.

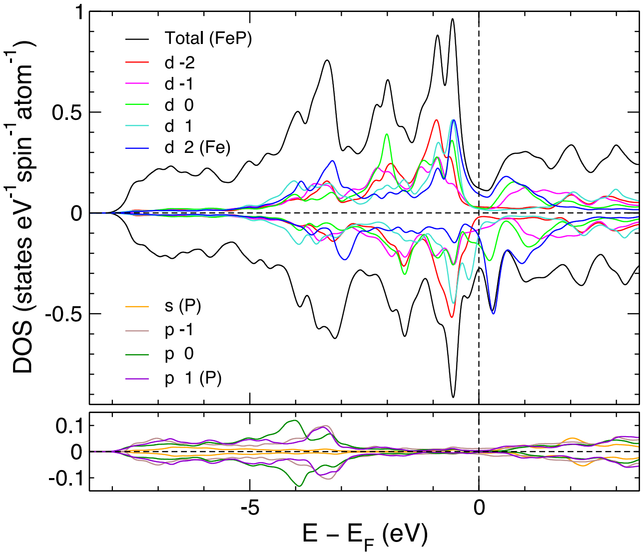

Figure S4. Electron DOS in bulk FeP, with spin-decomposed (majority (+) and minority (–)) and with l_m-decomposed DOS projected on 3*d* (Fe) and 3*s*, 3*p* (P) orbitals inside the atomic spheres.

Table S1. Computed surface energies relative to bulk FeP. The chosen low-energy termination of [201] surface can be viewed as [101](a) with periodic steps made by 2-atom wide [101](b) surface, see Figure S5. The other considered terminations of [201] were higher in energy.

Surface	Surface Energy (eV/Å^2)
[010]	0.1149
[111]*	0.1082*
[011]	0.0946
[101](a)	0.1025
[101](b)	0.1314
[201]	0.1317

* [111] surface is non-stoichiometric, the surface energy is provided for bulk stoichiometric 1:1 FeP forming the P-rich [111] surface and segregated bulk bcc Fe.

(a) (b) see surfaces in Figures S5a and S5b, respectively.

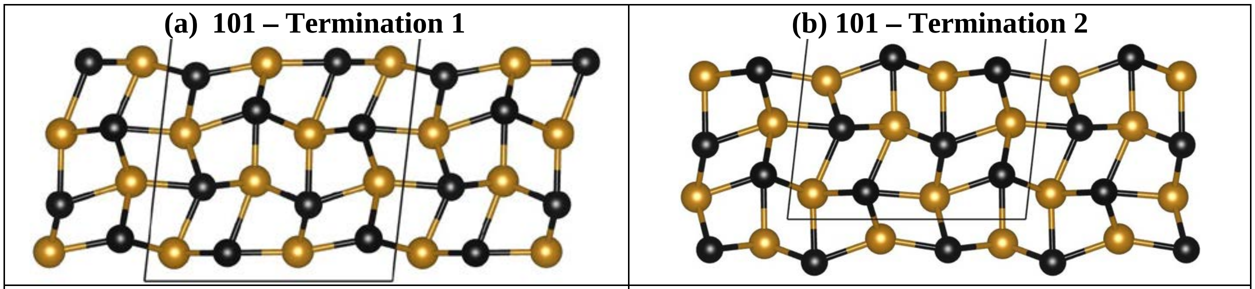

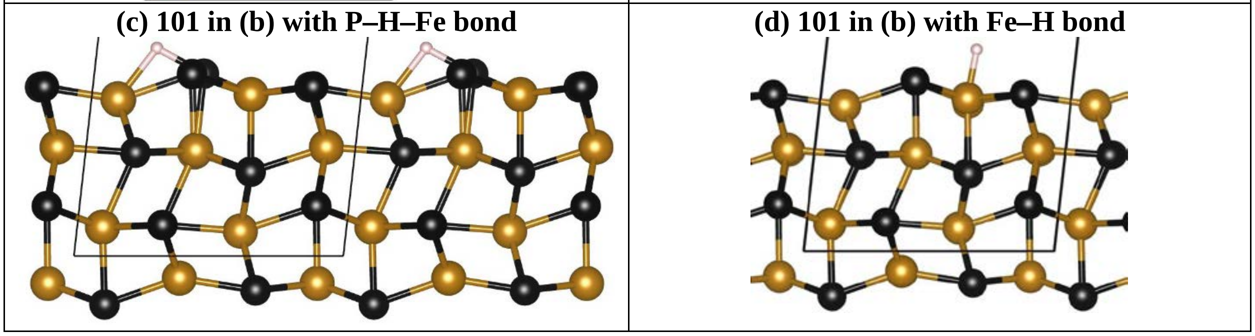

Figure S5. [101] surface terminations in 010 projection pf FeP. Atoms are denoted by spheres for Fe (orange), P (black), and H (white). Termination 1 (a) is +0.03 eV/A^2 higher in energy than termination 2 (b). For a H atom on [101] (b), the lowest-energy (–2.324 eV) is a bridge P–H–Fe position (c), as in Figure 6, while bonding to P or Fe (d) is less stable (–2.252 eV).

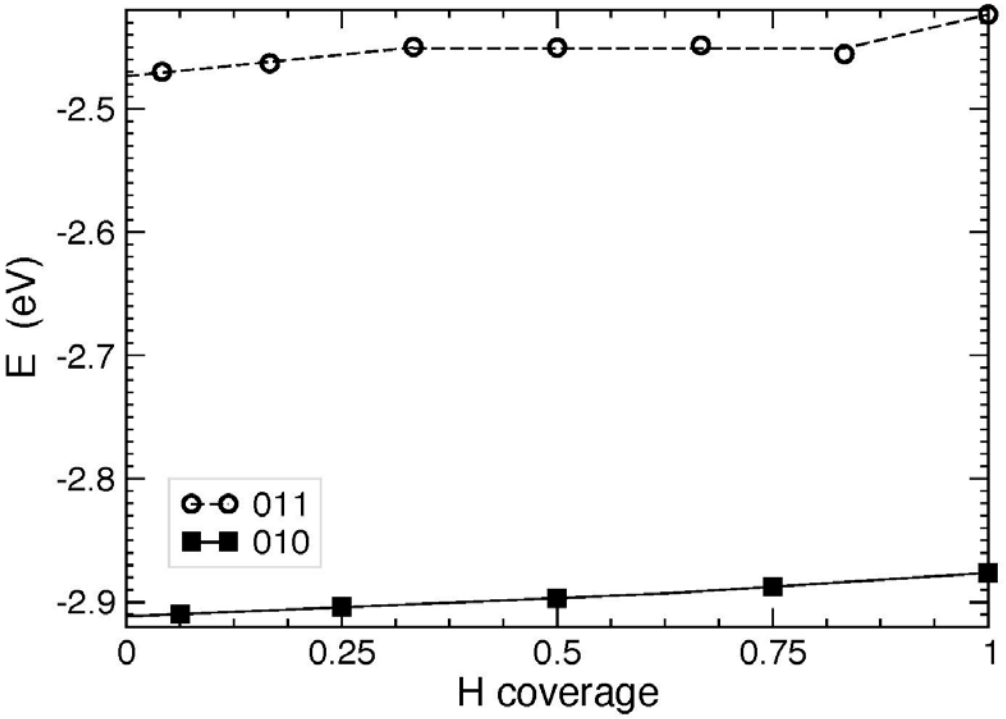

Figure S6. The variation of the H adsorption energies with H coverage for [010] and [011] FeP surfaces.

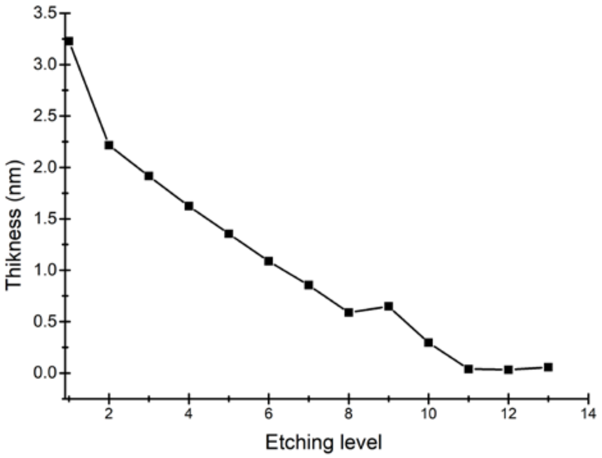

Figure S7. Estimated overlayer thickness during surface cleaning of the FeP sample by Ar cluster etching. The final etch cycles correspond to a clean FeP crystal surface (Figure 7c in the main text). The thickness of the oxidized overlayer was estimated based on the ratio of the oxidized (overlayer) and phosphide (bulk) P 2p components, following the methodology previously described and validated for chemically modified overlayers on crystalline compound semiconductors.[13,14]

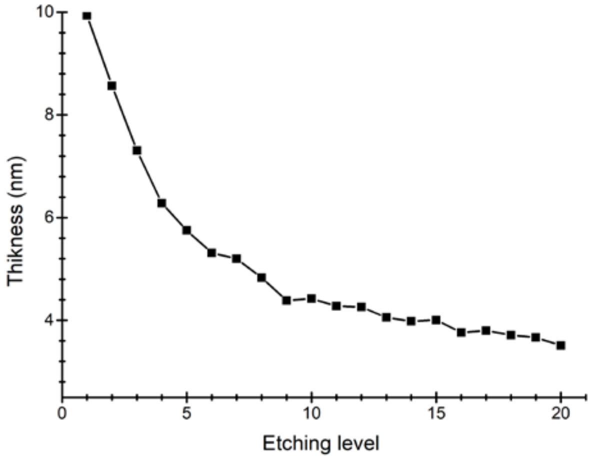

Figure S8. Estimated overlayer thickness during surface cleaning of the NiP_2 sample by Ar cluster etching. The etch rate clearly slowed down after ca. 10 etching cycles; oxidized overlayer (Figure 8c in the main text) of ca. 4 nm thickness remained even after approximately double the etching time used for the FeP sample.

References

1. Powell, C. J., Recommended Auger parameters for 42 elemental solids. *J. Electron. Spectrosc. Relat. Phenom.* **2012,** *185* (1), 1-3.
2. Wang, X.; Li, W.; Xiong, D.; Petrovykh, D. Y.; Liu, L., Bifunctional Nickel Phosphide Nanocatalysts Supported on Carbon Fiber Paper for Highly Efficient and Stable Overall Water Splitting. *Adv. Funct. Mater.* **2016,** *26* (23), 4067-4077.
3. Xu, J.; Sousa, J. P. S.; Mordvinova, N. E.; Costa, J. D.; Petrovykh, D. Y.; Kovnir, K.; Lebedev, O. I.; Kolen'ko, Y. V., Al-Induced In Situ Formation of Highly Active Nanostructured Water-Oxidation Electrocatalyst Based on Ni-Phosphide. *ACS Catal.* **2018,** *8* (3), 2595-2600.
4. Xu, J.; Wei, X.-K.; Costa, J. D.; Lado, J. L.; Owens-Baird, B.; Gonçalves, L. P. L.; Fernandes, S. P. S.; Heggen, M.; Petrovykh, D. Y.; Dunin-Borkowski, R. E.; Kovnir, K.; Kolen'ko, Y. V., Interface Engineering in Nanostructured Nickel Phosphide Catalyst for Efficient and Stable Water Oxidation. *ACS Catal.* **2017,** *7* (8), 5450-5455.
5. Bao, X.-Q.; Petrovykh, D. Y.; Alpuim, P.; Stroppa, D. G.; Guldris, N.; Fonseca, H.; Costa, M.; Gaspar, J.; Jin, C.; Liu, L., Amorphous oxygen-rich molybdenum oxysulfide Decorated p-type silicon microwire Arrays for efficient photoelectrochemical water reduction. *Nano Energy* **2015,** *16*, 130-142.
6. Owens-Baird, B.; Xu, J.; Petrovykh, D. Y.; Bondarchuk, O.; Ziouani, Y.; González-Ballesteros, N.; Yox, P.; Sapountzi, F. M.; Niemantsverdriet, H.; Kolen'ko, Y. V.; Kovnir, K., NiP2: A Story of Two Divergent Polymorphic Multifunctional Materials. *Chem. Mater.* **2019,** *31* (9), 3407-3418.
7. Petrovykh, D. Y.; Sullivan, J. M.; Whitman, L. J., Quantification of discrete oxide and sulfur layers on sulfur-passivated InAs by XPS. *Surf. Interface Anal.* **2005,** *37* (11), 989-997.
8. Stine, R.; Aifer, E. H.; Whitman, L. J.; Petrovykh, D. Y., Passivation of GaSb and InAs by pH-activated thioacetamide. *Appl. Surf. Sci.* **2009,** *255* (16), 7121-7125.
9. Cumpson, P. J.; Portoles, J. F.; Barlow, A. J.; Sano, N.; Birch, M., Depth profiling organic/inorganic interfaces by argon gas cluster ion beams: sputter yield data for biomaterials, in-vitro diagnostic and implant applications. *Surf. Interface Anal.* **2013,** *45* (13), 1859-1868.

10. Scofield, J. H., Hartree-Slater subshell photoionization cross-sections at 1254 and 1487 eV. *J. Electron. Spectrosc. Relat. Phenom.* **1976,** *8* (2), 129-137.
11. Jablonski, A.; Powell, C. J., The electron attenuation length revisited. *Surf. Sci. Rep.* **2002,** *47* (2), 33-91.
12. Tanuma, S.; Powell, C. J.; Penn, D. R., Calculations of electron inelastic mean free paths. V. Data for 14 organic compounds over the 50–2000 eV range. *Surf. Interface Anal.* **1994,** *21* (3), 165-176.
13. Petrovykh, D. Y.; Sullivan, J. M.; Whitman, L. J., Quantification of discrete oxide and sulfur layers on sulfur-passivated InAs by XPS. *Surf. Interface Anal.* **2005,** *37* (11), 989-997.
14. Stine, R.; Aifer, E. H.; Whitman, L. J.; Petrovykh, D. Y., Passivation of GaSb and InAs by pH-activated thioacetamide. *Appl. Surf. Sci.* **2009,** *255* (16), 7121-7125.